HHS Public Access

Author manuscript

Cytotherapy. Author manuscript; available in PMC 2024 April 29.

Published in final edited form as:

Cytotherapy. 2024 April ; 26(4): 372–382. doi:10.1016/j.jcyt.2024.01.009.

Scalable manufacture of therapeutic mesenchymal stromal cell products on customizable microcarriers in vertical wheel bioreactors that improve direct visualization, product harvest, and cost

Andrew Haskell[1], **Berkley P. White**[2], **Robert E. Rogers**[1], **Erin Goebel**[1,2], **Megan G. Lopez**[1], **Andrew E. Syvyk**[4], **Daniela A. de Oliveira**[4,5], **Heather A. Barreda**[1], **Joshua Benton**[1], **Oscar R. Benavides**[2], **Sujata Dalal**[1], **EunHye Bae**[1], **Yu Zhang**[1], **Kristen Maitland**[2,3], **Zivko Nikolov**[4,5], **Fei Liu**[1], **Ryang Hwa Lee**[1], **Roland Kaunas**[2,*], **Carl A. Gregory**[1,**]

[1]Department of Cell Biology and Genetics, Texas A&M School of Medicine, Bryan, Texas, USA

[2]Department of Biomedical Engineering, Texas A&M University, College Station, Texas, USA

[3]Imaging Program, Chan Zuckerberg Initiative, Redwood City, California, USA

[4]National Center for Therapeutics Manufacturing, Texas A&M University, College Station, Texas, USA

[5]Biological and Agricultural Engineering, Texas A&M University, College Station, Texas, USA

Abstract

Background aims: Human mesenchymal stromal cells (hMSCs) and their secreted products show great promise for treatment of musculoskeletal injury and inflammatory or immune diseases. However, the path to clinical utilization is hampered by donor-tissue variation and the inability to manufacture clinically relevant yields of cells or their products in a cost-effective manner. Previously we described a method to produce chemically and mechanically customizable gelatin methacryloyl (GelMA) microcarriers for culture of hMSCs. Herein, we demonstrate scalable GelMA microcarrier-mediated expansion of induced pluripotent stem cell (iPSC)-derived hMSCs (ihMSCs) in 500 mL and 3L vertical wheel bioreactors, offering several advantages over conventional microcarrier and monolayer-based expansion strategies.

*Correspondence: Roland Kaunas, Department of Biomedical Engineering, Texas A&M University, Emerging Technologies Building 3120, 101 Bizzell St, College Station, Texas, USA. **Correspondence: Carl A. Gregory, Department of Cell Biology and Genetics, Texas A&M School of Medicine, Bryan, Texas, 77807 USA, rkaunas@tamu.edu (R. Kaunas), cgregory@tamu.edu (C.A. Gregory).

Author Contributions

Conceptualization, AH, RER, KM, ZN, RL, RK, and CAG; Funding acquisition, KM, ZN, RK, and CAG; Methodology, AH, BPW, RER, EG, AES, DAO, RL, RK, and CAG; Investigation, AH, BPW, EG, MGL, AES, DAO, HAB, JB, ORB, SD, EB, and ZY; Supervision, KM, ZN, FL, RL, RK, and CAG, Project administration, AH, BPW, AES, RL, RK, and CAG, Writing — original draft, AH and CAG; Writing — review and editing, all authors.

Declaration of Competing Interest

The authors declare no competing interests.

Supplementary materials

Supplementary material associated with this article can be found in the online version at doi:10.1016/j.jcyt.2024.01.009.

Methods: Human mesenchymal stromal cells derived from induced pluripotent cells were cultured on custom-made spherical gelatin methacryloyl microcarriers in single-use vertical wheel bioreactors (PBS Biotech). Cell-laden microcarriers were visualized using confocal microscopy and elastic light scattering methodologies. Cells were assayed for viability and differentiation potential in vitro by standard methods. Osteogenic cell matrix derived from cells was tested in vitro for osteogenic healing using a rodent calvarial defect assay. Immune modulation was assayed with an in vivo peritonitis model using Zymozan A.

Results: The optical properties of GelMA microcarriers permit noninvasive visualization of cells with elastic light scattering modalities, and harvest of product is streamlined by microcarrier digestion. At volumes above 500 mL, the process is significantly more cost-effective than monolayer culture. Osteogenic cell matrix derived from ihMSCs expanded on GelMA microcarriers exhibited enhanced *in vivo* bone regenerative capacity when compared to bone morphogenic protein 2, and the ihMSCs exhibited superior immunosuppressive properties *in vivo* when compared to monolayer-generated ihMSCs.

Conclusions: These results indicate that the cell expansion strategy described here represents a superior approach for efficient generation, monitoring and harvest of therapeutic MSCs and their products.

Keywords

bioreactor; cell culture; gelatin methacryloyl microcarriers; mesenchymal stromal cells; stem cell manufacture; stem cell therapy

Introduction

Human mesenchymal stromal cells (hMSCs) and their secreted products are promising candidates for the development of broad-spectrum therapeutics owing to their ability to differentiate into connective tissues and the capacity to modulate the immune system [1–5]. For example, hMSCs from various tissue sources have the capacity to facilitate the repair of bone and cartilage in experimental models and in clinical trials [6–15] and the immunomodulatory properties of hMSCs also give them utility for treatment of inflammatory disorders such as rheumatoid arthritis, Chron's disease, and graft-vs-host disease [16–18]. Nevertheless, the translational impact of hMSC therapy is challenged by the unpredictable nature of tissue-derived hMSC batches yielding variable results in preclinical studies [19–22] and in clinical trials [23,24]. A committee of the International Society for Cell and Gene Therapy (ISCT), the society that established the minimal criteria for hMSC classification [25], recently reviewed clinical trials that tested hMSCs for the treatment for acute respiratory distress as a result of COVID-19. This review highlighted that the major determinants of variability in clinical trials are likely donor-derived variability and inconsistent manufacturing practices [26]. Recently, induced pluripotent stem cells (iPSCs) have been used to derive hMSCs, and the resultant iPSC-derived hMSCs (ihMSCs) have been reported to share the comparable differentiation and immune modulatory properties as tissue-derived hMSCs [27–31]. Utilizing iPSCs as a source for hMSCs mitigates variables pertaining to donor variability because iPSCs can be theoretically expanded without limit from a genetically identical source.

Culture of hMSCs has traditionally been achieved using plastic-adherent monolayer culture, with flasks, plates or multistack systems [32], but while these methodologies are well characterized, scale-up is labor and resource-intensive. In view of this, there has been a recent shift to microcarrier culture, motivated by a need to better facilitate cell yields required for widespread clinical use [33–36]. Cell-laden microcarriers can be cultured in spinner flasks but many therapeutic cell types are susceptible to the adverse effects of shear stresses caused by rapid fluid agitation [37]. To significantly reduce shear effects, rocking-bag cultures are available [38], but there are scale limitations with these systems. Vertical wheel bioreactors offer the same flexibility and scalability as stirred-tank bioreactors, but subject cell-laden microcarriers to less shear stress, representing a suitable compromise between scalability and agitation parameters for large-scale cell manufacture on microcarriers [39]. Current commercial microcarriers are primarily produced from plastic, ceramic or polysaccharide, often with a biocompatible coating such as collagen. Several commercially available microcarriers have been approved for the manufacture of various cell types, but they are nondegradable and must be filtered from the cells upon harvest which may result in shear stress, clogging of the filtration device, and kinetic damage to the cells [40,41].

The current challenge for the development of hMSC-derived technologies is the provision of the means to generate clinically relevant yields of hMSCs or their products in a manner that is safe, scalable, reproducible, biocompatible, and cost effective.

This group previously described an approach to fabricate customizable, degradable gelatin methacryloyl microcarriers (GelMA-M) using a step-emulsification microfluidic device [42]. The microcarriers exhibited improved optical characteristics as compared to their polystyrene counterparts [43] and simplified cell harvest by complete digestion of the microcarriers. When cultured on GelMA-M in vertical wheel bioreactors (VWB) at 100 mL scale, the ihMSCs retained in vitro trilineage differentiation potential and immune modulatory capacity [42]. In this study, we demonstrate that VWB/GelMA-M culture is scalable to at least 3L in a manner that is more cost effective than standard monolayer expansion. The GelMA-M permits accurate enumeration of attached ihMSCs by light sheet imaging of fluorescently labeled nuclei and label-free visualization of cell bodies by elastic light scattering microscopy (ELSM). Rapid product harvest is achieved by microcarrier digestion using standard trypsin-based cell dissociation reagents. In proof-of-concept studies performed in vivo, we demonstrate that the system can be used to generate ihMSC-derived osteogenic cellular matrix (OCM) or immunomodulatory ihMSCs.

Collectively, these results indicate that the VWB/GelMA-M cell expansion strategy described here represents a superior approach for efficient generation, monitoring and harvest of therapeutic MSCs and their products.

Results

Expansion of ihMSCs attached to GelMA-M in 500 mL VWBs.

GelMA-M spherical microcarriers were synthesized using the microfluidic approach we previously reported [42]. GelMA-M equivalent to 2500 cm^2 of growth area were cultured

with an initial seed of 2.5×10^6 ihMSCs in a single-use 500 mL VWB. Samples were recovered every 2 days for cell enumeration followed by replacement of 50% of the medium. Control cultures were performed as monolayers attached to tissue culture plates and with porcine gelatin-coated polystyrene microcarriers (Pall-Solohill) in 500 mL VWBs. These microcarriers were chosen because they share the biochemistry of GelMA-M microcarriers. After an initial 4-day lag phase, a rapid period of expansion on GelMA-M resulted in approximately 5 population doublings followed by a stationary period after day 6 of culture (Figure 1A,B). Expansion on monolayer culture was unremarkable, with cells gradually accumulating with increases in doubling time as cell density increased (Figure 1A,B). Expansion with VWB/GelMA-M plateaued at 30 000 cells per cm^2 (S.D. 2000) (yield 6.9×10^7–8.0×10^7), monolayer yields were significantly lower at 21 000 cells per cm^2 (S.D. 800) and cell yields using polystyrene microcarriers were 15 000 cells per cm^2 (S.D. 1500) (Figure 1A). Visualization of the microcarriers by confocal microscopy after fluorescent staining of cytoplasm and nuclei indicated the presence of live, intact cells attached to the surface of GelMA-M. Furthermore, the surface area on GelMA-M was completely occupied at day 6 with aggregation of the cell-laden microcarriers (Figure 1C, see supplementary Figure S1). We have previously demonstrated that elastic light scattering (ELS) can be employed to visualize the cytoplasm of cells attached to the surface of GelMA-M without need for fixation or labeling and with computational image analysis, this modality could be leveraged to enumerate cells [43]. When cell number measurements generated by ELS were compared to those determined by a hemacytometer-based automated cell counter, measurements correlated strongly (Pearson r, 0.9943, $P < 0.0005$) (Figure 1C). Cells attached to GelMA-M were recovered by digestion of the microcarriers by treatment with a standard trypsin-based dissociation reagent resulting in a final viability of over 95%. The ihMSCs then readily proliferated on standard monolayer plastic with a classic, spindle-shaped morphology [33]. When subjected to standard osteogenic assays in monolayer cultures, ihMSCs expanded by VWB/GelMA-M and polystyrene microcarriers both exhibited improved mineralization potential as compared to ihMCSs expanded on monolayers when measured by alizarin red S (ARS) staining followed by ARS recovery and spectrophotometric quantification (Figure 1D) [44]. Several studies have reported that ihMSCs exhibit poor adipogenic differentiation potential when using adipogenic differentiation medium (ADM) adapted for tissue-derived hMSCs [27,42]. When the dose of indomethacin and dexamethasone was raised 100-fold and 2-fold respectively (ADM*), adipogenic responses by ihMSCs were superior to use of standard ADM (see supplementary Figure S2A). An additional adipogenic induction protocol (AIM) originally adapted for brown adipocyte differentiation [45] was also tested but this had limited effect on ihMSCs (see supplementary Figure S2A). Adipogenic potential of ihMSCs grown on monolayer, polystyrene microcarriers and GelMA-M was compared by staining of lipid droplets with Oil Red O (ORO) followed by isopropanol extraction. With ADM*, polystyrene outperformed monolayer and GelMA-M derived ihMSCs, with GelMA-M ihMSCs generating the fewest lipid vacuoles. These results are expected given the inverse relationship between osteogenic and adipogenic propensities of MSCs [6]. Collectively, these data demonstrate that the 500 mL VWB/GelMA-M microcarrier system generates greater cellular yields than monolayer and polystyrene microcarriers and is suitable for scalable expansion of ihMSCs.

Scalability of cultures to 3 L.

Scalability is an attractive characteristic of PBS VWB systems. We questioned whether cultures could be scaled from 500 mL to 3 L without significant impact to yield. In the case of 500 mL bioreactors, the vessels are contained in standard humidified tissue culture incubators in the presence of 5% (v/v) CO_2 but the 3L bioreactors require aeration and CO_2 supply. To recapitulate conditions of monolayer culture and the 500 mL VWB as closely as possible, CO_2 flow was set to a constant delivery of 0.3 L min^{-1} resulting in a pH range of 7.0–7.5 for the duration of the culture. Dissolved oxygen was equivalent to atmospheric conditions, delivered by headspace aeration. A 500 mL VWB/GelMA-M culture was employed to generate the cells necessary to seed the 3L VWB. In contrast with the expansion kinetics observed with 500 mL bioreactors where the majority of cell accumulation occurred during a proliferative burst between day 4 and 6, proliferation in the 3L proceeded gradually with a relatively constant doubling time (Figure 2A,B). Yields were slightly lower than in monolayer cultures which exhibited a rapid phase of growth at day 2–4 with progressive lengthening of doubling time as the cultures approached the stationary phase. In this case, final yields were (20 500 cells per cm^2, S.D. 800) from monolayer cultures and 14 500 per cm^2 (S.D. 6500) for the 3L bioreactor with a final yield of 1.43×10^8–3.28×10^8 cells.

As seen with the 500 mL cultures, accumulation of cells on the GelMA-M microcarriers occurred concomitant with aggregation (Figure 2C, see supplementary Figure S3). ELS imaging and cell enumeration generated results that strongly correlated with standard cell counting techniques (Pearson r, 0.9700, $P = .0062$) (Figure 2C). The ihMSCs expanded in the 3 L bioreactors generated osteoblast- and adipocyte-like cells in monolayer assays (Figure 2D,E). Cells attached to GelMA-M were recovered by digestion of the microcarriers by treatment with standard trypsin-based dissociation reagents with a final viability of over 90%. When expanded on monolayers, the recovered ihMSCs readily proliferated with a classic, spindle-shaped morphology.

These results indicate that expansion of ihMSCs using VWB/GelMA-M is scalable at 500 mL to 3L with yields that are similar to those observed in monolayer cultures. In the case of 3L however, there is a slight reduction in yield as compared to monolayer suggesting extension of the duration of culture or optimization of oxygen provision might be beneficial. Noninvasive imaging by ELS, and recovery by microcarrier digestion is also feasible at this scale.

Generation of an osteogenic cell matrix with therapeutic potential using the VWB/GelMA-M approach—We have reported that an osteogenic cell matrix generated by monolayer-cultured ihMSCs (ihOCM) has the capacity to efficiently heal experimental bone defects [46]. To examine whether ihOCM could be generated and harvested at pilot scale using the VWB/GelMA-M approach, ihMSCs were cultured in 500 mL VWB vessels on GelMA-M the presence of an osteogenic basal media (OBM) containing the PPARγ inhibitor GW9662 [47] to trigger secretion of high levels of ihOCM. After 8 days of exposure to OBM, the ihOCM was recovered from the osteogenically enhanced ihMSCs (OEihMSCs) and microcarriers by detergent lysis, nuclease digestion, light trypsinization

and a series of chloroform and acetone washes using a technique previously described for monolayers [47]. The extraction process served to deplete cell structures, globular protein and the microcarriers while leaving the ihOCM components intact (Figure 3A). Control ihOCM was generated in the same manner from monolayers. The electrophoretic profiles of ihOCM generated on GelMA-M were similar to profiles of ihOCM extracted from monolayer cultures (Figure 3B). While the ihOCM is a complex mixture of potentially osteogenic factors, presence of collagen VI, XII and the putative collagen VI/XII bridging molecule transforming growth factor-beta-induced protein (TGFBI) have been shown to correlate with osteogenic activity [46]. All three of the factors were present in monolayer-derived and GelMA-M-derived ihOCM (Figure 3C). The ihMSCs from GelMA-M cultures reproducibly yielded more ihOCM than monolayers when standardized to growth area (Figure 3D,E).

The therapeutic potential of live OEihMSCs and the ihOCM generated from them under GelMA-M and monolayer conditions were compared using a standard calvarial defect model performed in immune compromised nude mice. For evaluation of live cells, 1×10^6 OEihMSCs, previously cultured in monolayers or on GelMA-M, were implanted in 4 mm diameter calvarial defects using clotted human plasma as a vehicle. The ihOCM preparations were also implanted in another cohort of mice so as to fill the volume of the defect. Positive controls consisting of gelatin foam (GF) soaked with 50 μg mL^{-1} bone morphogenic protein 2 (BMP2) and negative controls consisting of GF soaked in saline were also performed. After 4 weeks, the mice were humanely euthanized and calvarial bones were recovered for microcomputed tomographic (μCT) scanning and histology.

Microcomputed tomographic (μCT) scans were employed to perform calculations of defect closure (as percentage area) (Figure 4B, see supplementary Figure S4A), volumetric bone formation (Figure 4C, see supplementary Figure S4B, Figure S5), healing index (HI) where a value of 1 represents the volume of bone generated in the defect that is equivalent to the volume of bone in an anatomically equivalent region of interest (ROI) on the contralateral side of the cranium (Figure 4E, see supplementary Figure S4D, Figure S5), surface area to volume ratio (SVR, normalized to the contralateral side) (Figure 4D, see supplementary Figure S4C, Figure S6) and average bone thickness at the defect (Figure 4F, see supplementary Figure S4E). Monolayer- and VWB/GelMA-M-generated live OEihMSCs did not induce significantly more bone formation than GF alone (Figure 4A, C, and E, *blue plots*), resulting in marginal defect closure (Figure 4B, *blue plots*). Where bone had formed under these conditions, the structures were of inferior thickness (Figure 4F, *blue plots*) and high SVR, indicating sparsely distributed bone (Figure 4D, *blue plots*). In contrast, extensive bone had formed in the presence of BMP2-soaked GF (Figure 4C,E, and F, *green plot*) resulting in near complete defect closure in most cases (Figure 4B, *green plot*). In the case of ihOCM, the monolayer and VWB/GelMA-M-derived materials were comparable to each other and also BMP2 in terms of volumetric bone formation (Figure 4C, *red plots*), HI (Figure 4D, *red plots*), SVR (Figure 4D, *red plots*) and structure thickness (Figure 4F, *red plots*) but ihOCM generated from VWB/GelMA-M was more effective in achieving defect closure than ihOCM generated by monolayers (Figure 4B, *red plots*), suggesting that the VWB/GelMA-M remained more evenly distributed throughout the defect.

Overall, ihOCM from both monolayer and VWB/GelMA-M sources exhibited equivalent osteogenic activity to BMP2 in quantitative assays, but on closer inspection, histological distinctions were apparent (see supplementary Figure S7). The ihOCM-driven *de novo* bone was confined to the site of the defect and consisted of dense bony structures composed of interspersed patches of mature bone and primitive osteoid with interconnected patches of fibrous tissue. Bone marrow containing compartments were evident in bone generated by ihOCM from monolayer and VWB/GelMA-M, but were more frequent in specimens from the VWB/GelMA-M ihOCM treated group. Histological analysis of defects from GF and live ihMSC treated groups indicated primarily fibrous tissue (see supplementary Figure S7A,C,E), but sparsely distributed bone was evident, especially from OEihMSCs generated in VWB/GelMA-M cultures (see supplementary Figure S7E). Bone was abundant in BMP2-treated defects, but these bone masses frequently lacked sufficient structural integrity to remain intact during histological processing (e.g., see supplementary Figure S7B). Cavities in the BMP2-treated *de novo* bone were often larger than seen with ihOCM-treated counterparts (see supplementary Figure S7B, Figure S8) with frequent presence of erythrocytes and lymphocytes (see supplementary Figure S7B, *arrowed green and yellow respectively*). It was also noted that all mice from the BMP2 treatment group exhibited palpable bony growths that often extended away from the defect (see supplementary Figure S8A,B). The BMP2-driven growths consisted of a bony external layer with a fatty (see supplementary Figure S8A) or fibrous (see supplementary Figure S8B) internal region that was devoid of mature bone. On the other hand, *de novo* bone in ihOCM treated defects was confined to the site of the defect and it was often thicker than the surrounding calvarial bone, likely reflecting the dimensions of the original implant which was slightly thicker than the calvaria (see supplementary Figure S8C). In all cases, ihOCM generated robust bone tissue that exhibited morphology that was typical of newly formed bone.

Collectively, these data indicate that the VWB/GelMA-M approach is suitable for scalable generation of functional ihOCM with yields per unit growth area are higher than those attained by monolayer culture. Of added importance is the ability to utilize trypsin to destroy the microcarriers during downstream processing of ihOCM. The ihOCM generated comparable levels of *de novo* bone to the clinical gold standard, BMP2, but ihOCM-driven bone tissue was histologically more reminiscent of natural bone, lacking the cavitation, ectopic bone formation and fibrous accumulations often observed with BMP2 [48–51].

GelMA microcarrier culture enhances the immunomodulatory potential of ihMSCs in vitro.

To assess the immunomodulatory potential of hMSCs generated by the VWB/GelMA-M approach, a standard peritonitis assay was performed where mice were subjected to intraperitoneal (IP) administration of Zymozan A to induce sterile inflammation (Figure 5A) [52]. After 15 min, 2×10^6 ihMSCs harvested from monolayer cultures or 3 L GelMA-M cultures were also administered by the IP route. A control group received sterile PBS with no cells. After 6 h, the mice were humanely euthanized and immune cells and secreted factors were collected by peritoneal lavage. To assay for inflammatory response [52], lavage supernatant was assayed for levels of tumor necrosis factor-α (TNF-α), interleukin-6 (IL-6) and chemokine ligands 1 and 2 (CXCL1 and CXCL2) by enzyme linked immunosorbent assay (ELISA) and cells were stained for CD11b and Ly6G followed by enumeration

by flow cytometry to determine neutrophil invasion. Mice treated with monolayer-derived ihMSCs exhibited a slight tendency for reduced levels of peritoneal inflammatory factors, but no measurements were significantly lower than in the saline only control group. However, mice that received ihMSCs cultured on GelMA-M exhibited significantly reduced peritoneal neutrophil invasion as well as reduced levels of peritoneal TNF-α, IL-6, and CXCL2 (Figure 5B).

These results indicate that ihMSCs expanded using the VWB/GelMA-M approach have the capacity to reduce several key markers of inflammation in a simple murine model of peritonitis, suggesting that ihMSCs expanded by this scalable approach possess valuable anti-inflammatory properties.

Preliminary cost analysis of the VWB/GelMA-M expansion strategy.

Generation of MSCs for human trials is commonly achieved by monolayer culture within single or multistack plates or flasks. Even though monolayer culture has disadvantages, familiarity with this approach is favored over drawbacks related to cost, reagent burden, labor intensity and scalability limitations. To gain insight into potential cost benefits of the VWB/GelMA-M approach versus monolayer culture, the materials costs associated with both approaches were compared. Monolayer cultures in 150 cm^2 plates were compared to VWB/GelMA-M cultures performed at 100 mL—3 L scale. In the case of GelMA-M synthesis, it was assumed that all microfluidic components, surfactant, and oil are replaced at the beginning of a 40-h uninterrupted work cycle (compatible with the operations of a manufacturing facility), but oil and surfactant is recycled during each work cycle.

Under these conditions, it is estimated that 160 000 cm^2 of growth area can be generated at a cost of \$0.02/cm^2 (Table 1) using a single microfluidic device [42]. For comparison, the 15 cm culture plates used for monolayer controls in this study were purchased for \$0.03/cm^2, the polystyrene microcarriers were purchased for approximately \$0.05/cm^2 and commercial multistack systems cost approximately \$0.05/cm^2. With consideration of the costs associated with attachment substrate, bioreactors, medium utilization and other reagents, VWB/GelMA-M expansion reduces the culture cost by 30% at the 500 mL scale and 35% at the 3 L bioreactor scale as compared to monolayer culture when normalized to growth area (Table 2). Given that medium is a primary driver of cost in cell manufacturing processes, it is important to note that in these experiments, cell yields per mL of medium utilized (including replenishments over 8 days) was 30 700 cells per mL in monolayers and 31 400 cells per mL for the 3 L VWB cultures. Clinical trials using human MSCs for a variety of diseases report a dose of 1×10^6–1.2×10^7 cells/kg [16,53]. Assuming the minimum dose of 6.8×10^7 cells is needed for a 68 kg adult, VWB/GelMA-M culture has the capacity to reduce the cost of an iPS-MSC therapy by \$4800 USD per dose.

Discussion

Previously, we demonstrated that monodisperse spherical GelMA microcarriers (GelMA-M), with tunable diameter and stiffness, could be generated in large numbers using a microfluidic step emulsification device, and that these microcarriers could be utilized to expand ihMSCs in 100 mL miniature VWBs [42]. Attached cells could be rapidly

harvested by enzymatic degradation of the microcarriers dismissing the need for separation of cells and microcarriers that often negatively impacts yield and viability. Unlike plastic microcarriers, the GelMA-M permitted direct visualization and enumeration of attached cells using light sheet imaging of fluorescently labeled specimens and ELSM could be performed on cell-laden GelMA-M without need for fixation or labeling [43]. Given that the VWB/GelMA-M system exhibited promising characteristics for cell manufacture, the current study focused on scalability of the culture system for generation of therapeutically useful cells and cell-derived products. The primary rationale for utilization of the commercially available PBS-VWB system is a significant body of literature supporting the linear scalability of the system [39,54–56] and the availability of bioreactors with capacity ranging from 100 mL to 80 L. In this study, existing protocols for 100 mL cultures were scaled to 0.5 L and 3 L.

One of the most useful characteristics of microcarrier cultures is the capacity to maximize the ratio of attachment surface to volume of growth medium. In this study, a relatively low surface area to volume ratio (SVR) of 5 cm^2 per mL was utilized because it corresponds to the SVR commonly employed for monolayer cultures, and a major focus of this study was to perform meaningful comparisons with monolayer derived ihMSCs. Increasing the SVR can lower manufacturing costs by increasing the growth area while minimizing the need for expensive media components, and successful short-term culture of MSCs has been reported using SVRs above 5 (Table 3) [35,57–59]. Nevertheless, rapid nutrient depletion and accumulation of waste products can occur more readily as the SVR of the culture is increased, and nutrient deprivation coupled with waste accumulation can affect final product quality. Continuous harvest of bioreactor cultures has the advantage of maximizing yields from a single bioreactor, but this procedure has the potential to amplify intraculture variation in both population doublings and cell-density. Both of these parameters can have a profound effect on downstream functionality [19,20,60–62].

In contrast with culture systems that utilize a continuous growth surface, the kinetics of cell expansion in microcarrier bioreactors is complicated by the initial seeding density, how this affects the relative proportion of populated microcarriers at the time of seeding, and the ability of cells to migrate from one carrier to another. In our previous study utilizing 100 mL bioreactors, a seeding density of 1000 cells per cm^2 was found to be optimal for GelMA-M, with nearly 100% of the cells becoming attached to the microcarriers after 22 h of incubation [42]. While this is a lower seeding density than many reported studies utilizing VWBs and similar bioreactors, the lower seeding density reduces the size of seed cultures while generating competitive yields (Table 3). In this study, an initial seeding density of 1000 cells per cm^2 predicts occupation of approximately 50% of the microcarriers after the attachment phase, and direct visualization at day 2 of culture suggests this is the case (Figure 1C, Figure 2C). As local cell density increases, transfer from one microcarrier to another is then necessary to facilitate further expansion and account for the observed population of virtually all microcarriers at the time of harvest. It is unclear whether this is achieved primarily through the process of detachment and reattachment or through migration between aggregated microcarriers, but microcarrier association is very common during the logarithmic phase of expansion and thereafter (e.g. Figure 2C, day 4).

When expanded on monolayers, ihMSCs used in this study are usually seeded at an initial density of 500–1000 cells per cm^2 for homogeneous cell dispersal and rapid expansion [46] followed by harvest at 15 000–25 000 cells per cm^2 (5–6 population doublings). This density at harvest corresponds to 60–70% confluence so as to avoid impairment of proliferation rate, clonogenicity, and differentiation potential that can be caused by prolonged exposure to confluence [33]. After 8 days of culture, the final cell density of ihMSCs expanded in 3L VWB/GelMA-M was slightly lower than observed for monolayers (Figure 2A) at 14 500 cells per cm^2 (versus 20 500 per cm^2 for monolayers), but the doubling time remained comparatively low, suggesting that a single additional day of culture has the potential to result in yields equivalent to monolayers (Figure 2B). It should be noted that monolayers received a complete medium change every 48 h whereas the VWB received a half-replenishment of medium every 48 h so as to reduce the risk of further aggregation in low medium volumes, and it is possible that this could have affected the rate of cell expansion. In contrast, ihMSCs grown in 500 mL bioreactors exhibited a rapid growth phase between days 4 and 6 that plateaued on day 7 at 30 000 cells/cm^2 (Figure 1A) Despite growing to relatively high density for ihMSCs, differentiation capacity and further proliferative activity on monolayers observed during preparation of the differentiation assays was not perturbed. The discrepancies between the growth kinetics of ihMSCs expanded in 500 mL and 3 L is unclear because growth conditions (initial seeding density, SVR, pH, medium composition, O_2 concentration) were comparable between the two bioreactors. It should be noted, however, that seed cultures for the 3L VWB were generated in 500 mL VWB rather than monolayers, and this could play a factor in the initial growth kinetics in the 3L bioreactor, especially if the 500 mL seed cultures were exposed to a short duration of confluence.

The ability to rapidly monitor live cells attached to GelMA-M without need for labeling, fixation or other time-consuming invasive optical techniques represents major advantage over other commercial microcarriers. The improved optical characteristics arise from a refractive index that is nearly identical to growth media and saline [42,43] permitting, with light sheet imaging, rapid visualization of relatively large aggregates that frequently occur in microcarrier cultures. Using an algorithm we have described elsewhere [43], fluorescently stained nuclei were employed to enumerate attached ihMSCs with accuracy equivalent to cell counts performed on recovered samples (Figure 1C, Figure 2C). It should be noted however, that while ELS cannot yet be employed to accurately determine cell counts, it can be used to accurately measure cell volume and this was found to correlate closely with ihMSC cell number in VWB/GelMA-M cultures [43]. Therefore, with appropriate standardization, ELS may be utilized to directly enumerate cells in real time without need to fix or label specimens. Moreover, continuous monitoring by ELS could in turn inform on rapid adjustment of culture conditions and accurate timing of product recovery.

We previously demonstrated that ihOCM derived from the same line of ihMSCs used in this study has the capacity to repair critical-sized bone defects with efficacy at least equivalent to the clinical benchmark BMP2 [46]. Here, we demonstrated that the VWB/GelMA culture system facilitated the scalable synthesis of ihOCM that could be readily recovered from cells and microcarriers by a simple series of digestions and washes (Figure 3A–C). At scale, the process of ihOCM recovery could be performed directly in the bioreactor vessel

dismissing the need to manually scrape that material off the plastic growth surface for further processing as is the case with standard monolayers [47]. Simplification of the process by processing the cell-laden GelMA-M in a closed system resulted in greater yields when compared to standard monolayers (Figure 3E). The ihOCM generated by standard monolayers and GelMA-M culture induced deposition of a comparable amount of *de novo* bone in murine critical-sized defects as the clinical gold standard BMP2 [63,64] (Figure 4), suggesting an equivalent level of healing. However, further inspection of the bone stimulated by BMP2 highlighted several concerning characteristics not shared by the ihOCM-driven bone. All BMP2-treated animals exhibited a large palpable growth by the fourth week of recovery which was confirmed to be bone by μCT and histology. These growths extended far beyond the site of the defect (see supplementary Figure S7) and exhibited histological characteristics not typical of natural bone (see supplementary Figure S6). The resultant bone was morphologically aberrant as compared to ihOCM-driven bone, with prominent voids containing fatty marrow (see supplementary Figure S7A) and fibrous tissue (see supplementary Figure S7B). There was also a prevalence of lymphocyte-like cells in the BMP2-treated defects (see supplementary Figure S6B). On the other hand, bone generated by ihOCM was histologically normal, with thick trabecular structures composed of mature bone and osteoid with interspersed islands of normal marrow (see supplementary Figure S6D,F, Figure S7C). The observations made here resemble clinical reports of BMP2-induced side-effects including inflammation, [65,66], osteolysis and ectopic bone formation [48–50], bone voiding [51] and osteopenia [67]. Despite these risks, biologics like BMP-2 are often considered preferable to cytotherapies and cadaveric allografts due to risk of batch variation, immune reaction, and the fear of disease transmission [64,68]. In this study, live cells induced very limited bone formation, indicating that extracellular matrices derived from ihMSCs are not only superior in efficacy to live cells, but they also have a far lower potential for disease transmission because the processing methodologies include exposure to putative antimicrobial agents such as chloroform and acetone [47,69,70]. It should be noted that OCM purification and testing was performed with material generated only at the 500 mL scale due to resource limitations. Successful functionality of this material supports additional future studies with OCM generated at scales above 3L.

The ihMSCs used in this study have been demonstrated to inhibit tumor necrosis factor-α output by a macrophage-like cell line [46] and interferon-γ output by isolated murine splenocytes [42] when challenged by lipopolysaccharide *in vitro*. To evaluate the potential anti-inflammatory effects of the VWB/GelMA-M generated ihMSCs, we employed a simple *in vivo* assay based on peritoneal inflammation induced by zymosan exposure followed by administration of ihMSCs by the same route [52]. Assay of peritoneal lavage demonstrated that ihMSCs generated by VWB/GelMA-M, but not monolayer, was sufficient to inhibit several markers of inflammation. The lack of activity by monolayer ihMSCs is surprising because live cells and their secreted extracellular vesicles (EV) have been shown to inhibit inflammation in various studies [71,72], but the improved performance of VWB/GelMA-M ihMSCs could be attributable to microcarrier culture which can improve EV output and immune modulatory capacity [73].

In this study, we hypothesized that degradable GelMA-M are well-suited for scale up of ihMSC cultures in VWBs. Using the standardized culture conditions (medium composition,

SVR, ambient O_2, physiological pH) GelMA-M attachment permitted robust expansion in VWBs from 100 mL [42] up to 3 L with lower cost of cell production at the 500 mL and 3 L scale relative to conventional monolayer culture. Uniquely, the process could be monitored by visualization of live cells while attached to the microcarriers using ELS. Two potentially therapeutic products were successfully generated using the VWB/GelMA-M system, OCM and immune modulatory ihMSCs. Given that the PBS VWB systems are designed for linear scalability, further scale up is feasible [39,54–56], but it should be noted that the 3 L bioreactors represent excellent suitability for personalized, autologous applications. While the approaches described herein offer several attractive advantages such as improved cost at scale, ease of product harvest, visualization, and the potential for chemical and biomechanical tuning of the microcarriers, this study has some limitations. At the 3L scale, cell recoveries were lower than those attained at 500 mL and on monolayers. Since a stationary phase was not attained during the 8-day culture duration, it is likely that extension of the culture time would improve yield. The 3 L bioreactors were also fed oxygen via headspace aeration rather than direct administration of O_2 in an attempt to maintain continuity in conditions between monolayers and 500 mL cultures. The pH remained stable in 3L cultures suggesting that severe hypoxia was not occurring in the cultures. Nevertheless, the potential benefits of direct O_2 administration should be addressed in further studies, especially in anticipation of further scale-up.

A preliminary cost analysis predicts that the generation of MSCs using the VWB/GelMA-M system could be more cost effective than monolayer expansion of cells. However, it should be noted that these results are based on limited data and account only for the materials utilized to generate the product. At this time, it is unclear how labor costs and time will factor into the production of GelMA-M and the cell-based products derived from them, and further work is required to determine more accurate assessments of cost effectiveness.

Given the need for robust, cost-effective modalities for the manufacture of cell-based products, the VWB/GelMA-M approach described here addresses several of the pain-points that currently challenge cell manufacture. It is robust, linearly scalable, utilizes standard conditions, permits rapid visualization of live cells, and is cost effective as compared to monolayer-based expansion.

Materials and Methods

For detailed methodology, refer to supplemental materials

Study design: The objective of this study was to determine whether GelMA-M microcarriers could be employed to expand ihMSCs or their ECM for immune modulation and bone regeneration. For all experiments, the number of replicates and statistical test used are reported in the figure legends. The reported replicates refer to biological replicates. All in vitro experiments in the main text were performed at least twice, and no outliers were excluded. For *in vivo* experiments, mice were randomly assigned to treatment groups. Group sizes were determined by power analyses using post hoc data sets to attain a power of 0.8 (α=0.05).

GelMA synthesis: GelMA was synthesized as previously described [42,74]

Microfluidic Device Fabrication and GelMA-Microcarrier (GelMA-M) Generation: Fabrication of the microcarrier generation microfluidic device and GelMA-M has been described in detail previously [42].

Monolayer Culture: Cell culture protocols were adapted from [33].

500 mL Bioreactor Culture: Passage 3 ihMSCs were expanded on monolayers prior to culture in 500 mL bioreactors. Seed cultures were assayed for viability and cell attachment to GelMA-M as described previously [75]. In each case, viability and attachment was above 90%. Two and one half million ihMSCs were added to a 500 mL single use PBS bioreactor module (PBS Biotech catalog#FA 0.5-D-001) containing 500 mL of CCM and 5.5×10^6 microcarriers (corresponding to 2500 cm^2 growth area, 1000 cells per cm^2, 0.5 cm^2 per mL medium). The bioreactor was placed in a humidified CO_2 (5.0%) incubator at 37°C. To facilitate attachment of ihMSCs to GelMA-M, the culture was mixed for 1 min at 12 RPM followed by static incubation for 20 min. After 24 h, the bioreactor base was set to 17 RPM continuously. The cultures were half-fed every 2 days. On day 8, the cell-laden GelMA-M were recovered by centrifugation at 500 RCF for 5 min and incubated with to 50 mL trypsin-EDTA for 5 min at 37°C. The trypsin was deactivated by addition of 100 mL CCM, followed by recovery of ihMSCs by centrifugation at 500 RCF for 5 min.

3 L Bioreactor Culture: The bioreactor vessel (PBS-3 Vertical-Wheel Single-Use Vessel (Floored Wheel catalog#FA-3-D-504) was prepared in accordance with manufacturer protocols for standard utilization. 1.5×10^7 ihMSCs were mixed with 3.3×10^7 microcarriers suspended in 1 L of 37°C CCM. To homogeneously attach ihMSCs to GelMA-M, a looped protocol was employed to agitate the culture at 20 RPM for 1 min followed by a 20-min pause. After 24 h, the vertical wheel was set to run continuously at 20 RPM. The culture was half-fed every 2 days. On day 8, the cell-laden GelMA-M were recovered on a 740 μm nylon mesh filter and washed thoroughly with PBS. Trypsin was added to the filter and after 8 min of digestion, an equal volume of CCM used to deactivate the trypsin followed by recovery of ihMSCs by centrifugation at 500 RCF for 5 min.

Microcarrier Imaging: Imaging was performed as previously described [43] using a Z1 Lightsheet microscope. ELS was achieved at 638 nm.

Osteogenic Differentiation: Reagents were purchased from Sigma Aldrich unless otherwise stated. Differentiation and staining with alizarin red and spectrophotometric quantification was performed as previously described [44,47].

Adipogenic Differentiation Potential: Reagents were acquired from Sigma Aldrich unless otherwise stated. Adipogenic differentiation was performed on ihMSC monolayers using three test formulations of adipogenic differentiation media (see Supplemental Materials). At the conclusion of differentiation, cultures were stained with Oil Red O, imaged and the dye was quantified spectrophotometrically (see Supplemental Materials).

ihOCM Generation: The ihOCM was extracted as previously described [47]. The cell-laden GelMA-M and monolayer slurry were resuspended in lysis buffer (0.1% (v/v) Triton

X-100, 1 mM $MgCl_2$, and 10 μg/mL DNAse I) and incubated at 37°C for 2 h on an orbital shaker at 60 RPM. After the initial incubation, 0.01% (v/v) trypsin was added and incubation was continued for 15 h. The ihOCM was then washed twice in dH_2O, once in chloroform, once in dH_2O, and once in acetone and then air-dried. Dry ihOCM was stored at −80°C until use.

Calvarial Defect Assay: All vertebrate animal procedures were performed in accordance with a protocol approved by the Texas A&M University Institutional Animal Care and Use Committee (IACUC) as described previously [46] and in the Supplemental Materials.

μCT Analysis: Fixed calvaria were rinsed with PBS and wrapped in parafilm (VWR International) immediately prior to scanning. 360° scans were conducted every 0.5° with a 22 kV, 166 mA beam at 18 μm resolution with automatic flat-field correction and frame averaging. NRecon (Micro Photonics) was used for axial reconstructions with 1% smoothing kernel gaussian, 5% beam hardening, and dynamic range of 0–0.146173. Misalignment compensation was performed automatically for each sample. A defect was drilled into the contralateral side of a fixed sample not used for analysis to standardize reconstruction and thresholding settings and mock hydroxyapatite phantoms (Bruker) were used to calibrate the instrument and analysis software. A standardized volume of interest was generated based on the dimensions of the mock defect in CTan (Micro Photonics) to calculate the volume and density of the *de novo* bone in the defect. CTvol (Micro Photonics) was used to render the scans, again using the mock defect to determine the threshold for new bone.

Histology: Blocks were embedded in paraffin, sectioned and stained in the standard manner with Masson's Trichrome Stain by the Research Histology Unit at the Texas A&M School of Veterinary and Biological Sciences.

Immunomodulation Assay: Two-month-old male BALB/c mice (Jackson Laboratories) were utilized in in accordance with a protocol approved by the Texas A&M University IACUC to perform a sterile peritonitis assay [52].

Statistics: GraphPad Prism version 9.4.1 for Windows was used for plotting data and performing statistical tests. Details of each statistical analysis are provided in figure legend

Supplementary Material

Refer to Web version on PubMed Central for supplementary material.

Acknowledgements

The authors would like to acknowledge Dr. Jing Dai and Dr. Arum Han for their support in developing the original versions of the microfluidic device used for microcarrier fabrication and the Texas A&M College of Veterinary Medicine Histology Laboratory for sectioning and staining the calvarial defects. The authors acknowledge Dr. Holly Gibbs and the Texas A&M Microscopy and Imaging Center for support and access to microscopy resources.

Funding

This work was funded by an X-Grant from the Texas A&M President's Excellence Fund (CAG, RK, RL, KM, ZN) and in part by an R01 Award from the National Institute of Arthritis and Musculoskeletal and Skin Diseases

R01AR066033 (CAG, RK) and a collaborative award from the National Science Foundation CBET-1264848 (RK) and CBET-1264832 (CAG).

References

[1]. Andrzejewska A, Lukomska B, Janowski M. Concise review: mesenchymal stem cells: from roots to boost. Stem Cells 2019;37(7):855–64. [PubMed: 30977255]

[2]. Prockop DJ. The exciting prospects of new therapies with mesenchymal stromal cells. Cytotherapy 2017;19:1–8. [PubMed: 27769637]

[3]. Prockop DJ, Prockop SE, Bertoncello I. Are clinical trials with mesenchymal stem/progenitor cells too far ahead of the science? Lessons from experimental hematology. Stem Cells 2014;32:3055–61. [PubMed: 25100155]

[4]. Liao H, Chung C, Huang CF, Chen H. Potential of using infrapatellar-fat-pad-derivedmesenchymal stem cells for therapy in degenerative arthritis: chondrogenesis, exosomes, and transcription regulation. Biomolecules 2022;12(3):386. [PubMed: 35327578]

[5]. Zha K, Sun Z, Yang Y, Chen M, Gao C, Fu L, et al. Recent developed strategies for enhancing chondrogenic differentiation of MSC: impact on MSC-based therapy for cartilage regeneration. Stem Cells International 2021;2021:8830834.

[6]. Zeitouni S, Krause U, Clough BH, Halderman H, Falster A, Blalock D, et al. Human mesenchymal stem cell-derived matrices for enhanced osteoregeneration. Sci Transl Med 2012;4:132ra155.

[7]. Crowley C, Wong JM, Fisher DM, Khan WS. A systematic review on preclinical and clinical studies on the use of scaffolds for bone repair in skeletal defects. Curr Stem Cell Res Ther 2013;8:243–52. [PubMed: 23317473]

[8]. Gerami MH, Khorram R, Rasoolzadegan S, Mardpour S, Nakhaei P, Hashemi S, et al. Emerging role of mesenchymal stem/stromal cells (MSCs) and MSCs-derived exosomes in bone- and joint-associated musculoskeletal disorders: a new frontier. Eur J Med Res 2023;28:86. [PubMed: 36803566]

[9]. Cuomo AV, Virk M, Petrigliano F, Morgan EF, Lieberman JR. Mesenchymal stem cell concentration and bone repair: potential pitfalls from bench to bedside. J Bone Joint Surg Am 2009;91:1073–83. [PubMed: 19411455]

[10]. Bruder SP, Kurth AA, Shea M, Hayes WC, Jaiswal N, Kadiyala S, et al. Bone regeneration by implantation of purified, culture-expanded human mesenchymal stem cells. J Orthop Res 1998;16:155–62. [PubMed: 9621889]

[11]. Mankani MH, Kuznetsov SA, Wolfe RM, Marshall GW, Robey PG. In vivo bone formation by human bone marrow stromal cells: reconstruction of the mouse calvarium and mandible. Stem Cells 2006;24:2140–9. [PubMed: 16763200]

[12]. Arinzeh TL, Peter SJ, Archambault MP, van den Bos C, Gordon S, Kraus K, et al. Allogeneic mesenchymal stem cells regenerate bone in a critical-sized canine segmental defect. J Bone Joint Surg Am 2003;85:1927–35. [PubMed: 14563800]

[13]. Killington K, Mafi R, Mafi P, Khan W. A systematic review of clinical studies investigating mesenchymal stem cells for fracture non-union and bone defects. Curr Stem Cell Res Ther 2018;13(4):284–91. [PubMed: 28914208]

[14]. Sinclair KL, Mafi P, Mafi R, Khan WS. The use of growth factors and mesenchymal stem cells in orthopaedics: in particular, their use in fractures and non-unions: a systematic review. Curr Stem Cell Res Ther 2017;12:312–25. [PubMed: 27306399]

[15]. Gomez-Barrena E, Padilla-Eguiluz N, Rosset P, Gebhard F, Hernigou P, Baldini N, et al. Early efficacy evaluation of mesenchymal stromal cells (MSC) combined to biomaterials to treat long bone non-unions. Injury 2020;51(Suppl. 1):S63–73.

[16]. Parekkadan B, Milwid JM. Mesenchymal stem cells as therapeutics. Ann Rev Biomed Eng 2010;12:87–117. [PubMed: 20415588]

[17]. Ghoryani M, Shariati-Sarabi Z, Tavakkol-Afshari J, Ghasemi A, Poursamimi J, Mohammadi M. Amelioration of clinical symptoms of patients with refractory rheumatoid arthritis following treatment with autologous bone marrow-derived mesenchymal stem cells: A successful clinical trial in Iran. Biomed Pharmacother 2019;109:1834–40. [PubMed: 30551438]

[18]. Panés J, Garcia-Olmo D, Assche GV, Colombel JF, Reinisch W, Baumgart DC, et al. Expanded allogeneic adipose-derived mesenchymal stem cells (Cx601) for complex perianal fistulas in Crohn's disease: a phase 3 randomised, double-blind controlled trial. Lancet 2016;388:1281–90. [PubMed: 27477896]

[19]. Phinney DG. Biochemical heterogeneity of mesenchymal stem cell populations: clues to their therapeutic efficacy. Cell Cycle 2007;6:2884–9. [PubMed: 18000405]

[20]. Jansen BJ, Gilissen C, Roelofs H, Schaap-Oziemlak A, Veltman JA, Raymakers RA, et al. Functional differences between mesenchymal stem cell populations are reflected by their transcriptome. Stem Cells Dev 2010;19:481–90. [PubMed: 19788395]

[21]. Qadan MA, Piuzzi NS, Boehm C, Bova W, Moos M Jr., Midura RJ, et al. Variation in primary and culture-expanded cells derived from connective tissue progenitors in human bone marrow space, bone trabecular surface and adipose tissue. Cytotherapy 2018;20:343–60. [PubMed: 29396254]

[22]. Lobo SE, Glickman R, da Silva WN, Arinzeh TL, Kerkis I. Response of stem cells from different origins to biphasic calcium phosphate bioceramics. Cell Tissue Res 2015;361:477–95. [PubMed: 25676006]

[23]. van der Spoel TIG, Jansen of Lorkeers SJ, Agostoni P, van Belle E, Gyongyosi M. Human relevance of pre-clinical studies in stem cell therapy: systematic review and meta-analysis of large animal models of ischaemic heart disease. Cardiovasc Res 2011;91:649–58. [PubMed: 21498423]

[24]. von Bahr L, Sundberg B, Lonnies L, Sander B, Karbach H, Hagglund H, et al. Long-term complications, immunologic effects, and role of passage for outcome in mesenchymal stromal cell therapy. Biol Blood Marrow Transplant 2012;18:557–64. [PubMed: 21820393]

[25]. Dominici M, Le Blanc K, Mueller I, Slaper-Cortenback I, Marini FC, Krause DS, et al. Minimal criteria for defining multipotent mesenchymal stromal cells. The International Society for Cellular Therapy position statement. Cytotherapy 2006;8:315–7. [PubMed: 16923606]

[26]. Weiss DJ, Filiano A, Galipeau J, Khoury M, Krampera M, Lalu M, et al. An International Society for Cell and Gene Therapy Mesenchymal Stromal Cells Committee editorial on overcoming limitations in clinical trials of mesenchymal stromal cell therapy for coronavirus disease-19: time for a global registry. Cytotherapy 2022;24:1071–3. [PubMed: 36028438]

[27]. Zhao Q, Gregory CA, Lee RH, Reger RL, Qin L, Hai B, et al. MSCs derived from iPSCs with a modified protocol are tumor-tropic but have much less potential to promote tumors than bone marrow MSCs. Proc Natl Acad Sci USA 2014;112:530–5. [PubMed: 25548183]

[28]. Villa-Diaz LG, Brown SE, Liu Y, Ross AM, Lahann J, Parent JM, et al. Derivation of mesenchymal stem cells from human induced pluripotent stem cells cultured on synthetic substrates. Stem Cells 2012;30:1174–81. [PubMed: 22415987]

[29]. Zhao C, Ikeya M. Generation and applications of induced pluripotent stem cell-derived mesenchymal stem cells. Stem Cells Int 2018;2018:9601623.

[30]. Hynes K, Menicanin D, Mrozik K, Gronthos S, Bartold PM. Generation of functional mesenchymal stem cells from different induced pluripotent stem cell lines. Stem Cells Dev 2014;23:1084–96. [PubMed: 24367908]

[31]. Kang R, Zhou Y, Tan S, Zhou G, Aagaard L, Xie L, et al. Mesenchymal stem cells derived from human induced pluripotent stem cells retain adequate osteogenicity and chondrogenicity but less adipogenicity. Stem Cell Res Ther 2015;6:144. [PubMed: 26282538]

[32]. Rowley J, Abraham E, Campbell A, Brandwein H, Oh SJBI. Meeting lot-size challenges of manufacturing adherent cells for therapy. Bioprocess Int 2012;10:7.

[33]. Gregory CA, Prockop DJ, in Culture of human stem cells, Freshney RI, Stacey GN, Averback JM, editor. (John Wiley & Sons, Hoboken, NJ, 2007 207–232.

[34]. Mizukami A, Chilima TDP, Orellana MD, Neto MA, Covas DT, Farid SS, et al. Technologies for large-scale umbilical cord-derived MSC expansion: experimental performance and cost of goods analysis. Biochem Eng J 2018;135:36–48.

[35]. de Sousa Pinta D, Bandeiras C, de Almeida Fuzeta M, Rofrigues CAV, Jung S, Hashimura Y, et al. Scalable manufacturing of human mesenchymal stromal cells in the vertical-wheel bioreactor system: an experimental and economic approach. Biotechnol J 2019;14(8):e1800716.

[36]. Simaria AS, Hassan S, Varadaraju H, Rowley J, Warren K, Vanek P, et al. Allogeneic cell therapy bioprocess economics and optimization: single-use cell expansion technologies. Biotechnol Bioeng 2013;111:69–83. [PubMed: 23893544]

[37]. Jossen V, Schirmer C, Mostafa Sindi D, Eibl R, Kraume M, Portner R, et al. Theoretical and practical issues that are relevant when scaling Up hMSC microcarrier production processes. Stem Cells Int 2016;2016:4760414.

[38]. Wierzchowski K, Pilarek M. Disposable rocking bioreactors: recent applications and progressive perspectives. Trends Biotechnol 2023. S0167–7799(23)00277–9.

[39]. de Sousa Pinto D, Bandeiras C, de Almeida Fuzeta M, Rodrigues CAV, Jung S, Hashimura Y, et al. Scalable manufacturing of human mesenchymal stromal cells in the vertical-wheel bioreactor system: an experimental and economic approach. Biotechnol J 2019;14:e1800716.

[40]. Chuna B, Peixoto C, Silva MM, Carrondo MJT, Serra M, Alves PM. Filtration methodologies for the clarification and concentration of human mesenchymal stem cells. J Membr Sci 2015;478:117–29.

[41]. Moloudi R, Oh S, Yang C, Teo KL, Lam ATL, Warkiani ME, et al. Inertial-based filtration method for removal of microcarriers from mesenchymal stem cell suspensions. Sci Rep 2018;8(1):12481. [PubMed: 30127526]

[42]. Rogers RE, Haskell A, White BP, Dalal S, Lopez M, Tahan D, et al. A scalable system for generation of mesenchymal stem cells derived from induced pluripotent cells employing bioreactors and degradable microcarriers. Stem Cells Transl Med 2021;10:1650–65. [PubMed: 34505405]

[43]. Benavides OR, Gibbs HC, White BP, Kaunas R, Gregory CA, Walsh AJ, et al. Volumetric imaging of human mesenchymal stem cells (hMSCs) for non-destructive quantification of 3D cell culture growth. PLoS One 2023;18:e0282298.

[44]. Gregory CA, Gunn WG, Peister A, Prockop DJ. An Alizarin red-based assay of mineralization by adherent cells in culture: comparison with cetylpyridinium chloride extraction. Anal Biochem 2004;329:77–84. [PubMed: 15136169]

[45]. Townsend KL, An D, Lynes MD, Huang TL, Zhang H, Goodyear LJ, et al. Increased mitochondrial activity in BMP7-treated brown adipocytes, due to increased CPT1- and CD36-mediated fatty acid uptake. Antioxid Redox Signal 2013;19:243–57. [PubMed: 22938691]

[46]. McNeill EP, Zeitouni S, Pan S, Haskell A, Cesarek M, Tahan D, et al. Characterization of a pluripotent stem cell-derived matrix with powerful osteoregenerative capabilities. Nat Commun 2020;11:3025. [PubMed: 32541821]

[47]. Gregory CA, McNeill EP, Pan S. Preparation of osteogenic matrices from cultured cells. Methods Cell Biol 2020;156:15–43. [PubMed: 32222217]

[48]. Lewandrowski KU, Nanson C, Calderon R. Vertebral osteolysis after posterior interbody lumbar fusion with recombinant human bone morphogenetic protein 2: a report of five cases. Spine J 2007;7:609–14. [PubMed: 17526434]

[49]. Chrastil J, Low JB, Whang PG, Patel AA. Complications associated with the use of the recombinant human bone morphogenetic proteins for posterior interbody fusions of the lumbar spine. Spine (Phila Pa 1976) 2013;38:E1020–7. [PubMed: 23629484]

[50]. Tannoury CA, An HS. Complications with the use of bone morphogenetic protein 2 (BMP-2) in spine surgery. Spine J 2014;14:552–9. [PubMed: 24412416]

[51]. Flouzat-Lachaniette CH, Ghazanfari A, Bouthors C, Poignard A, Hernigou P, Allain J. Bone union rate with recombinant human bone morphogenic protein-2 versus autologous iliac bone in PEEK cages for anterior lumbar interbody fusion. Int Orthop 2014;38:2001–7. [PubMed: 24627122]

[52]. Lee RH, Yu JM, Foskett AM, Peltier G, Reneau JC, Bazhanov N, et al. TSG-6 as a biomarker to predict efficacy of human mesenchymal stem/progenitor cells (hMSCs) in modulating sterile inflammation in vivo. Proc Natl Acad Sci U S A 2014;111:16766–71. [PubMed: 25385603]

[53]. Galipeau J, Sensébe L. Mesenchymal stromal cells: clinical challenges and therapeutic opportunities. Cell Stem Cell 2018;22:824–33. [PubMed: 29859173]

[54]. Borys BS, So T, Colter J, Dang T, Roberts EL, Revay T, et al. Optimized serial expansion of human induced pluripotent stem cells using low-density inoculation to generate clinically

relevant quantities in vertical-wheel bioreactors. Stem Cells Transl Med 2020;9:1036–52. [PubMed: 32445290]

[55]. Neto PM, Nogueira DES, Hashimura Y, Jung S, Pedras B, Berberan-Santos MN, et al. Characterization of the aeration and hydrodynamics in vertical-wheel bioreactors. Bioengineering (Basel) 2022;9(8):386. [PubMed: 36004911]

[56]. de Almeida Fuzeta M, Bernardes N, Oliveira FD, Costa AC, Fernandes-Platzgummer A, Farinha JP, et al. Scalable production of human mesenchymal stromal cell-derived extracellular vesicles under serum-/xeno-free conditions in a microcarrier-based bioreactor culture system. Front Cell Dev Biol 2020;8:553444. [PubMed: 33224943]

[57]. Jeske R, Liu C, Duke L, Castro MLC, Muok L, Arthur P, et al. Upscaling human mesenchymal stromal cell production in a novel vertical-wheel bioreactor enhances extracellular vesicle secretion and cargo profile. Bioact Mat 2022;25:732–47.

[58]. Lawson T, Kehoe DE, Schnitzler AC, Rapiejko PJ, Der KA, Philbrick K, et al. Process development for expansion of human mesenchymal stromal cells in a 50 L single-use stirred tank bioreactor. Biochem Eng J 2017;120:49–62.

[59]. Lembong J, Kirian R, Takacs JD, Olsen TR, Lock LT, Rowley JA, et al. Bioreactor parameters for microcarrier-based human MSC expansion under xeno-free conditions in a vertical-wheel system. Bioengineering 2020;7(3):73. [PubMed: 32650422]

[60]. Gregory CA, Ylostalo J, Prockop DJ. Adult bone marrow stem/progenitor cells (MSCs) are preconditioned by microenvironmental “niches” in culture: a two-stage hypothesis for regulation of MSC fate. Sci STKE 2005;2005:pe37.

[61]. Larson BL, Ylostalo J, Lee RH, Gregory C, Prockop DJ. Sox11 is expressed in early progenitor human multipotent stromal cells and decreases with extensive expansion of the cells. Tissue Eng Part A 2010;16:3385–94. [PubMed: 20626275]

[62]. Sekiya I, Larson BL, Smith JR, Pochampally R, Cui JG, Prockop D. J.Expansion of human adult stem cells from bone marrow stroma: conditions that maximize the yields of early progenitors and evaluate their quality. Stem Cells 2002;20:530–41. [PubMed: 12456961]

[63]. de Grado GF, Keller L, Indoux-Gillet Y, Wagner Q, Musset A, Benkirane-Jessel N, et al. Bone substitutes: a review of their characteristics, clinical use, and perspectives for large bone defects management. J Tissue Eng 2018;9. 2041731418776819.

[64]. Lobb DC, DeGeorge BR, Chhabra AB. Bone graft substitutes: current concepts and future expectations. J Hand Surg 2019;44(6):497–505.

[65]. Neovius E, Lemberger M, Docherty Skogh AC, Hilborn J, Engstrand T. Alveolar bone healing accompanied by severe swelling in cleft children treated with bone morphogenetic protein-2 delivered by hydrogel. J Plast Reconstr Aesthet Surg 2013;66:37–42. [PubMed: 22980542]

[66]. Smucker JD, Rhee JM, Singh K, Yoon ST, Heller JG. Increased swelling complications associated with off-label usage of rhBMP-2 in the anterior cervical spine. Spine (Phila Pa 1976) 2006;31:2813–9. [PubMed: 17108835]

[67]. Toth JM, Wang M, Patel CK, Arora A. Early term effects of rhBMP-2 on pedicle screw fixation in a sheep model: histomorphometric and biomechanical analyses. J Spine Surg 2018;4:534–45. [PubMed: 30547116]

[68]. Ibrahim T, Stafford H, Esler CNA, Power RA. Cadaveric allograft microbiology. Int Orthop 2004;28:315–8. [PubMed: 15480661]

[69]. Dyrda G, Boniewska-Bernacka E, Man D, Barchiewicz K, Slota R. The effect of organic solvents on selected microorganisms and model liposome membrane. Mol Biol Rep 2019;46:3225–32. [PubMed: 30937654]

[70]. Bunyea H. Adaptation of the bacterial action of chloroform to the preparation of bacterins. J Agric Res 1927;34:623–30.

[71]. Yu Y, Wang D, Li H, Fan J, Liu Y, Zhao X, et al. Mesenchymal stem cells derived from induced pluripotent stem cells play a key role in immunomodulation during cardiopulmonary resuscitation. Brain Res 2019;1720:146293. [PubMed: 31201814]

[72]. Bertolino GM, Maumus M, Jorgensen C, Noel D. Recent advances in extracellular vesicle-based therapies using induced pluripotent stem cell-derived mesenchymal stromal cells. Biomedicines 2022;10(9):2281. [PubMed: 36140386]

[73]. Kim H, Lee MJ, Bae EH, Ryu JS, Kaur G, Kim HJ, et al. Comprehensive molecular profiles of functionally effective MSC-derived extracellular vesicles in immunomodulation. Mol Ther 2020;28(7):1628–44. [PubMed: 32380062]

[74]. Loessner D, Meinert C, Kaemmerer E, Martine LC, Yue K, Lavett PA, et al. Functionalization, preparation and use of cell-laden gelatin methacryloyl-based hydrogels as modular tissue culture platforms. Nat Protoc 2016;11:727–46. [PubMed: 26985572]

[75]. Rogers RE, Haskell A, White BP, Dalal S, Lopez M, Tahan D, et al. A scalable system for generation of mesenchymal stem cells derived from induced pluripotent cells employing bioreactors and degradable microcarriers. Stem Cells Transl Med 2021;10(12):1650–65. [PubMed: 34505405]

[76]. Dos Santos F, Campbell A, Fernandes-Platzgummer A, Andrade PZ, Gimble JM, Wen Y, et al. A xenogeneic-free bioreactor system for the clinical-scale expansion of human mesenchymal stem/stromal cells. Biotechnol Bioeng 2014;111:1116–27. [PubMed: 24420557]

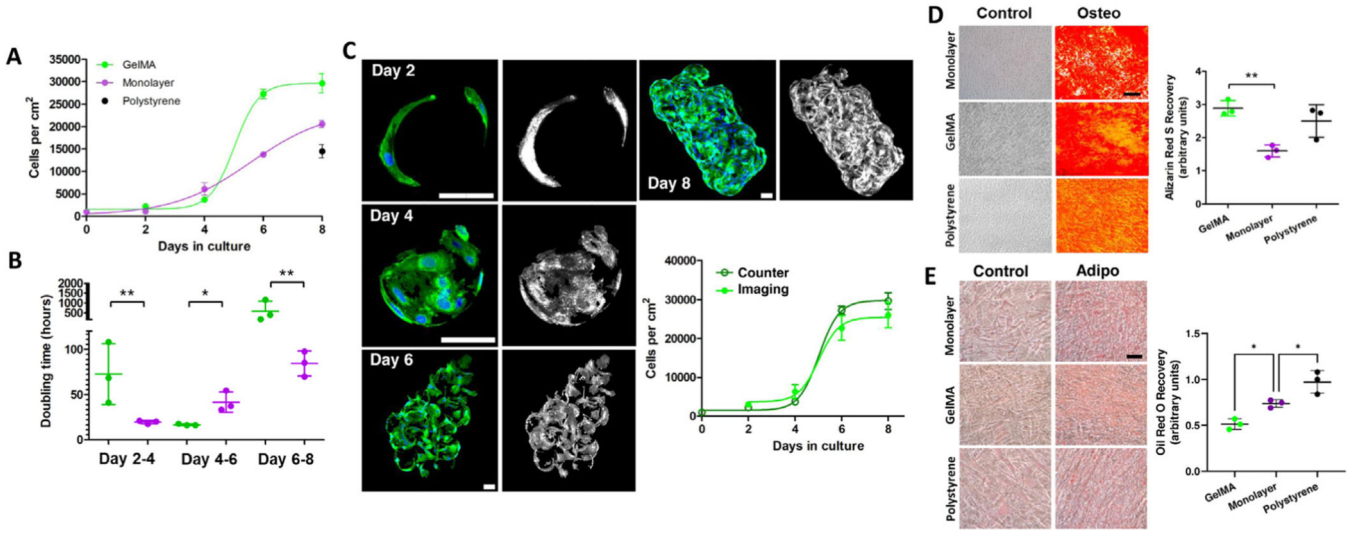

Figure 1.

Expansion of ihMSCs in 500 mL vertical wheel bioreactors. (A) Growth curves (n=3) for ihMSCs cultured on GelMA-M in 500 mL VWBs (*green*) compared to 15 cm monolayer culture plates (*purple*). Final yield for polystyrene microcarriers (*black*). Error bars represent standard deviations. (B) Doubling times at specified durations of culture for ihMSCs cultured on GelMA -M (*green*) compared to monolayers (*purple*). Horizontal line represents the mean and error bars represent standard deviations. Data analyzed by Student's *t*-test. Asterisks represent * = $P < 0.05$, ** = $P < 0.01$. (C) Merged DiO (*green*) and DRAQ5 (*blue*) staining of ihMSCs growing on GelMA-M and images generated by elastic light scattering (*monochrome*) (*bar* = 50 μm). Also refer to supplementary Figure S1. Comparison of cell enumeration by standard cell counts compared to results generated by analysis of fluorescent light sheet images (*below right*). (D) *In vitro* osteogenic differentiation of ihMSCs cultured on monolayers and GelMA-M. Representative phase contrast images (*left*) of undifferentiated (*Control*) and differentiated cells (*Osteo*) stained with Alizarin Red S (*bar* = 200 μm). Quantification of ARS staining in differentiated cultures (*right*). Data analyzed by ANOVA and Tukey post-test. Asterisks represent ** = $P < 0.01$. (E) *In vitro* adipogenic differentiation of ihMSCs cultured on monolayers and GelMA-M. Representative phase contrast images of undifferentiated (*Control*) and differentiated cells (*Adipo*) stained with Oil Red O (*bar* = 100 μm). Quantification of ARS staining in differentiated cultures (*right*). Horizontal line represents the mean and error bars represent standard deviations. Data analyzed by ANOVA and Tukey post-test. Asterisk represents * = $P < 0.05$.

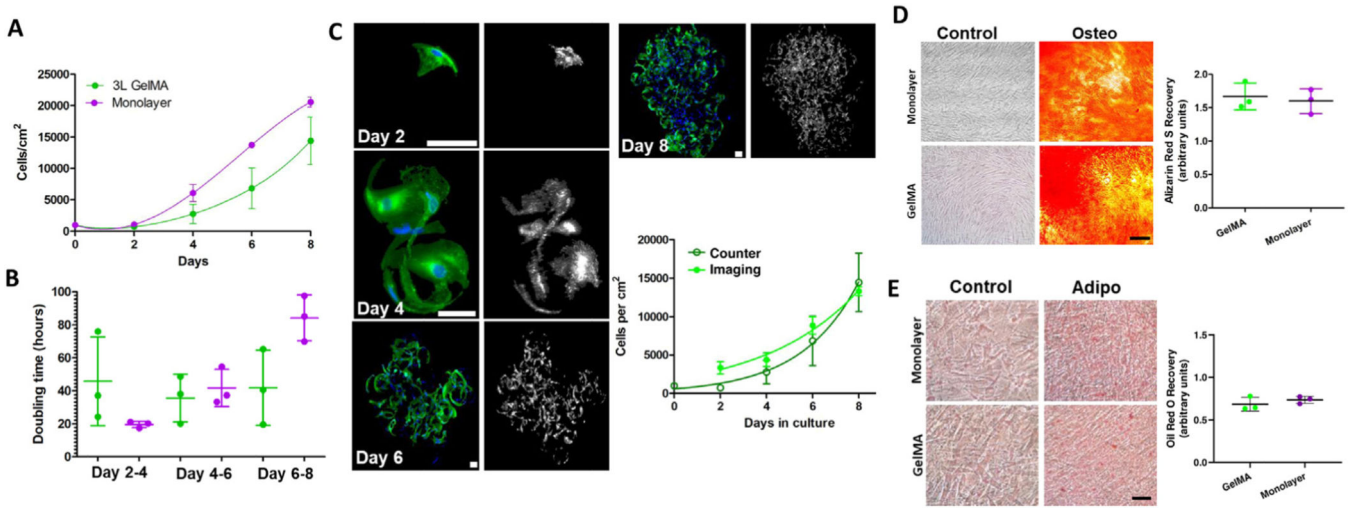

Figure 2.

Expansion of ihMSCs on GelMA microcarriers in 3L vertical wheel bioreactors. (A) Growth curves (n=3) for ihMSCs cultured on GelMA-M in 3 L vertical wheel bioreactors (*green*) compared to 15 cm monolayer culture plates (*purple*). Error bars represent standard deviations. (B) Doubling times at specified durations of culture for ihMSCs cultured on GelMA-M (*green*) compared to monolayers (*purple*). Horizontal line represents the mean and error bars represent standard deviations. Data analyzed by Student's *t*-test. (C) Merged DiO (*green*) and DRAQ5 (*blue*) staining of ihMSCs growing on GelMA-M and images generated by ELSM (*monochrome*) (*bar* = 50 μm). Also refer to supplementary Figure S7. Comparison of cell enumeration by standard cell counts compared to results generated by analysis of fluorescent light sheet images (*below right*). (D) *In vitro* osteogenic differentiation of ihMSCs cultured on monolayers and GelMA-M. Representative phase contrast images (*left*) of undifferentiated (*Control*) and differentiated cells (*Osteo*) stained with Alizarin Red S (*bar* = 200 μm). B) Quantification of ARS staining in differentiated cultures (*right*). Data analyzed by ANOVA and Tukey post-test. (E) *In vitro* osteogenic differentiation of hMSCs cultured on monolayers and GelMA-M. Representative phase contrast images of undifferentiated (*Control*) and differentiated cells (*Adipo*) stained with Oil Red O (*bar* = 200 μm). For (D and E), horizontal line represents the mean and error bars represent standard deviations. Asterisks represent * = $P < 0.05$, ** = $P < 0.01$, *** = $P < 0.005$.

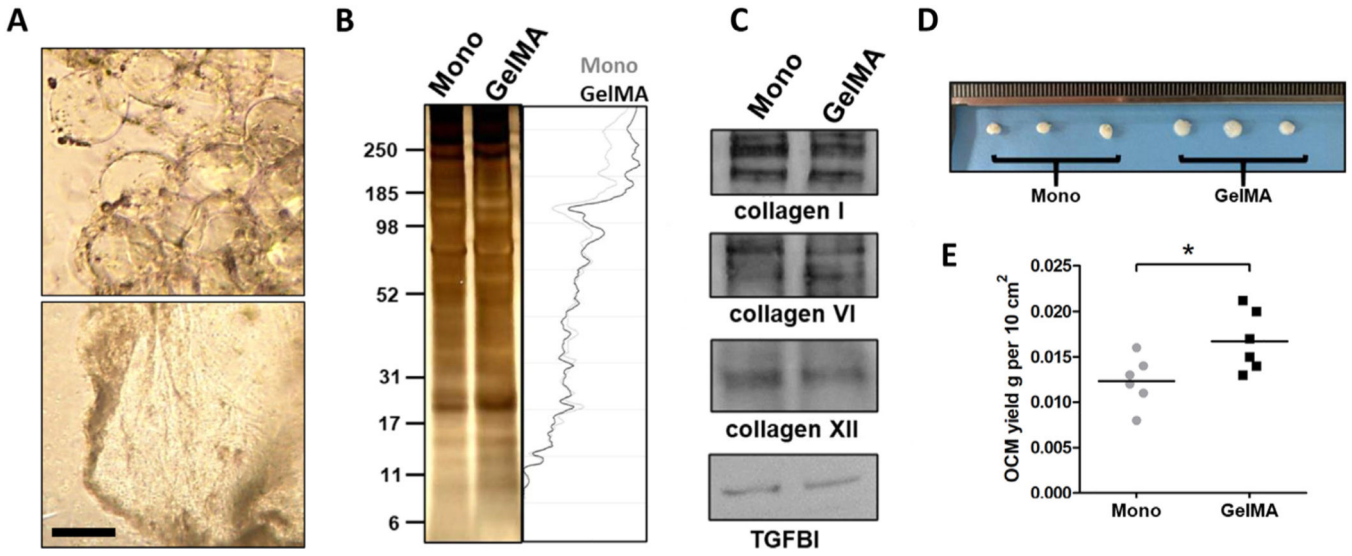

Figure 3.

Growth of iPS-hMSCs on GelMA microcarriers improves yields and simplifies recovery of ihOCM. (A) Phase contrast images of osteogenically enhanced ihMSCs and ihOCM attached to microcarriers (*above*), ihOCM after decellularization and digestion of microcarriers (*below*) (*bar* = 100 μm). (B) Silver stained SDS-PAGE electropherogram of ihOCM generated from iPSC-OEhMSCs cultured on monolayers (*Mono*) and gelMA-M (*GelMA*). Densitometry trace is provided on right. Each lane was loaded with 50 μg of material. (C) Immunoblots for key ihOCM components collagen I, VI and XII and TGFBI using conditions identical to Panel B. (D, E) Recovery of ihOCM from 10 cm2 of growth area on monolayers or GelMA-M shown in pure pelleted form (D) with mass quantification (E). Horizontal bar represents the mean. Data analyzed by Student's *t*-test, * = $P < 0.05$.

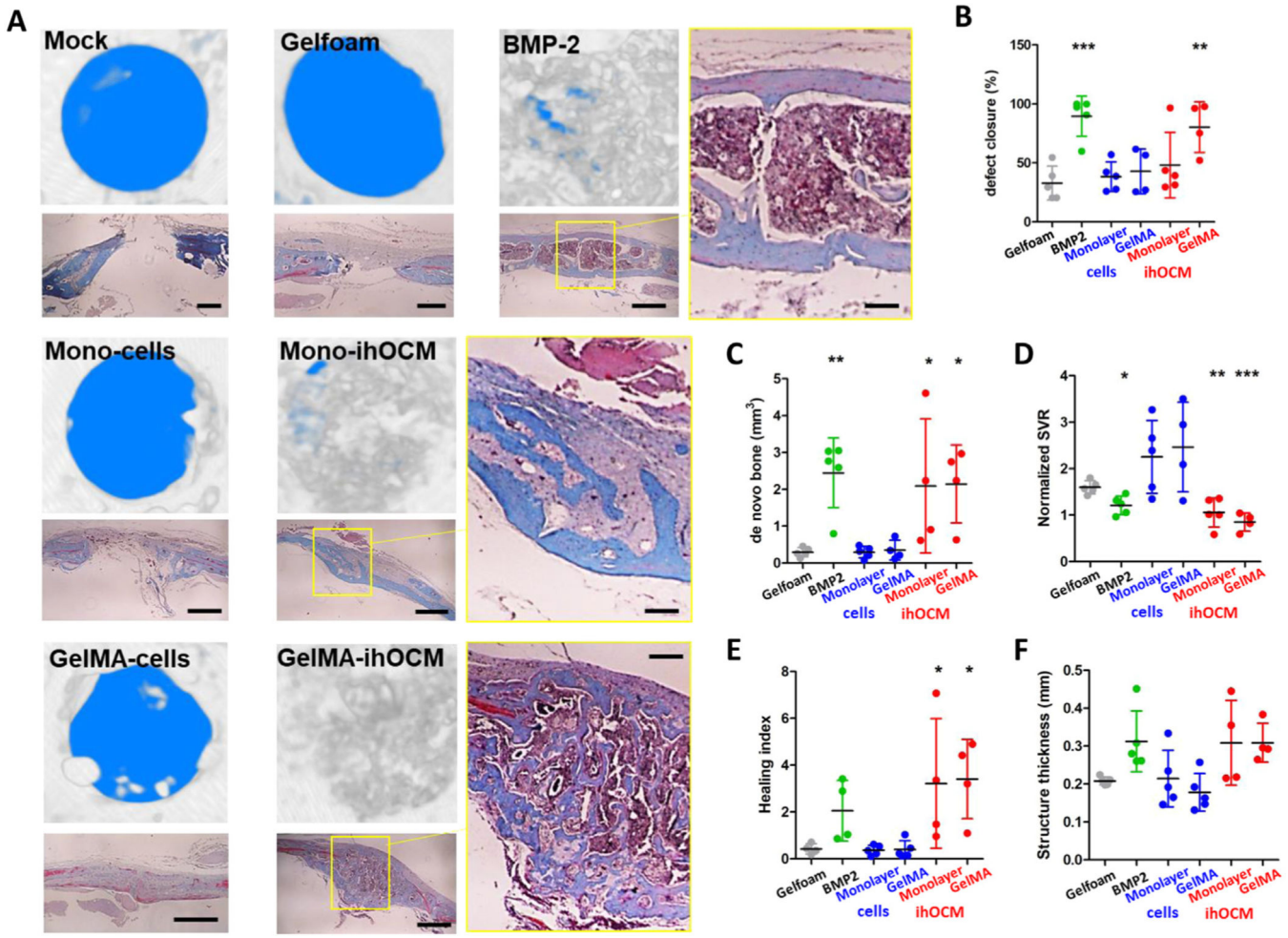

Figure 4.

The ihOCM generated on GelMA microcarriers heal critical-sized calvarial bone defects. (A) Three-dimensional renderings of calvarial defects after 4 weeks of healing in the presence of no material (*Mock*), Gelfoam, BMP-2, osteogenically enhanced ihMCS grown as standard monolayers (*Mono-cells*) or GelMA-M (*GelMA-cells*) and ihOCM generated from standard monolayers (*Mono-ihOCM*) or from GelMA-M (*GelMA-ihOCM*). Trichrome-stained histological sections are presented below each rendering (*bar* = 1 mm) with high power magnification for BMP-2 and ihOCM at right of panel (*bar* = 200 μm). (B) Defect closure as a function of percent defect filled by bone tissue. (C) Volume of *de novo* bone formed at site of defect. (D) SVR normalized to an anatomically equivalent region on contralateral side. (E) Healing index as a function of the ratio between the volume of *de novo* bone at the defect normalized to an anatomically equivalent region on contralateral side. (F) Average structure thickness of *de novo* bone. In each case, horizontal line represents the mean and error bars represent standard deviations. Results analyzed by one-way ANOVA and Dunnett's multiple comparison test with Gelfoam as the control. Asterisks represent * = $P < 0.05$, ** = $P < 0.01$, *** = $P < 0.005$. Also refer to Figures S2–5.

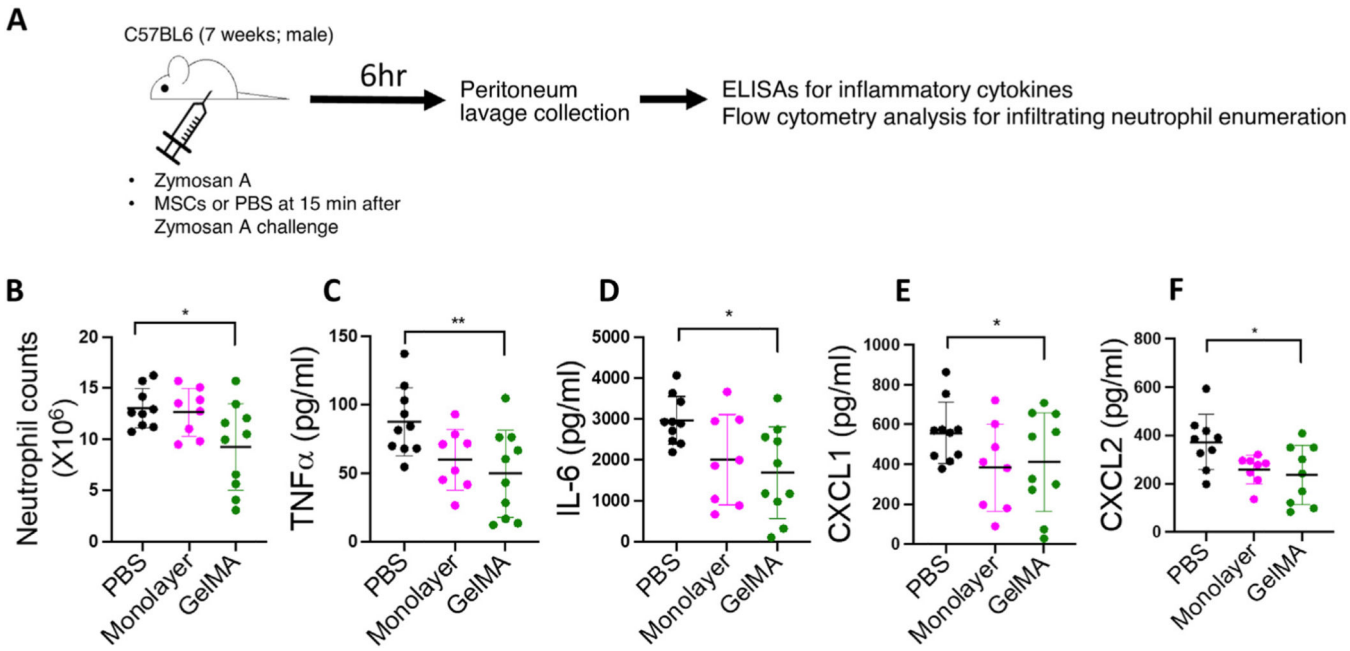

Figure 5.

ihMSCs harvested from GelMA-M exhibit immunomodulatory characteristics *in vivo*. (A) Mice were subjected to peritoneal challenge with zymosan followed by administration of PBS containing ihMSCs. After 5 h peritoneal lavages were subjected to measurements of inflammatory markers. (B) Proportion of cells collected from peritoneal lavage positive for neutrophil markers CD11b and Ly6G. (C–F) Levels of TNF-α, IL-6, CXCL1, or CXCL2 in peritoneal lavages as determined by ELISA. All measurements are presented as a percentage normalized to PBS. Results are analyzed by one-way ANOVA with Tukey's multiple comparison test, n = 10, * = $P < 0$.

Table 1

Estimated weekly cost to produce GelMA microcarriers at the current scale.

Running costs per week			
Component	**Amount/day (day 1)**	**Amount/day(days 2–5)**	**Cost ($)**
Photo initiator (g)	0.188	0.188	$126.90
Needles	2	0	$9.80
0.02” Tubing (ft)	5	0	$19.33
PDMS (g)	10	0	$20.86
Slides	1	0	$6.77
Fluorinated oil (mL)	104	31.2	$567.42
Surfactant (mL)	26	7.8	$2230.80
0.01” Tubing (ft)	5	0	$18.63
Gelatin (g)	24	24	$23.98
Glycerol (mL)	120	120	$51.00
Methacrylic anhydride (mL)	6	6	$4.54
PBS (mL)	1000	1000	$211.70
	Total cost/week ($)	$3291.73	
Product per week			
Microcarriers	354000000		
Growth area (cm^2)	160008		
Cost/cm^2 ($)	$0.02057		

Represents fabrication using a single setup running for 8 h per day, 5 days per week. Assumes all-new components are used on day 1% and 70% of surfactant/fluorinated oil are retained on each subsequent day.

Cytotherapy. Author manuscript; available in PMC 2024 April 29.

Table 2

Scale-up as it relates to cell production costs.

Culture parameters				Liquid usage			Cost						
Vol (mL)	**SA (cm^2)**	**GelMA (cm^2)**	**Cells produced**[1]	**Medium (mL)**[2]	**Trypsin (mL)**	**PBS (mL)**	**Bioreactor**[3]	**Medium**	**Trypsin**	**PBS**	**GelMA**[4]	**Cost/culture**	**Cost/10^6 cells**
25	150	0	1350000	130	4	5	$5.00	$268.44	$0.65	$0.21	$0.00	$274.29	**$203.18**
100	500	500	4500000	525	10	20	$220.50	$1084.07	$1.61	$0.85	$10.00	$1317.03	**$292.67**
500	2500	2500	22500000	1375	50	60	$288.75	$2839.24	$8.07	$2.54	$50.00	$3188.59	**$141.72**
3000	15000	15000	135000000	7975	170	1000	$990.00	$16467.58	$27.42	$42.34	$300.00	$17827.34	**$132.05**

[1] Not including seed cells.

[2] Medium used in this report contains 10% fetal bovine serum costed at good manufacturing practice grade.

[3] Bioreactors refer to standard Corning 150 cm diameter plate or single use vertical wheel bioreactor vessels (PBS Biotech).

[4] Refer to Table 1.

The cost to generate 1×10^6 ihMSC cells are calculated for monolayer culture using 150 cm^2 flasks (top row) and compared to vertical wheel bioreactor culture cells attached to GelMA microcarriers at 100 mL, 500 mL, and 3000 mL scale. Calculations exclude common consumables and overhead expenses. Calculations based on a final cell density of 10000 cells/cm^2 from an initial seeding density of 1000 cells/cm^2.

Table 3

Summary of bioreactor culture conditions and yields reported in literature.

Cell line	Surface area (cm^2)	Volume (mL)	SVR cm^2/mL	Initial Cells	Seeding density (cells/cm^2)	Yield	Final density (cells/cm^2)	Fold change	Cells/mL	Days	<REF> Reference PMID or DOI)
iPS-MSC[2]	500	100	5	500000	1000	6571000	13142	26.284	65710	8	herein
iPS-MSC[2]	500	100	5	500000	1000	6301 750	12603.50	25.207	62393.60	8	[38]
iPS-MSC[2]	2500	500	5	2500000	1000	74030000	29612	59.224	148060	8	herein
iPS-MSC[2]	2500	500	5	2500000	1000	36233 250	14493.30	28.9866	72466.50	8	[38]
iPS-MSC[2]	15000	3000	5	15000000	1000	328290000	14432	28.864	109430	8	herein
UCM-MSC[2]	720	100	7.2	4999 680	6944	53000000	73611.10	147.2222	530000	8	[39]
adMSC[2]	720	100	7.2	4999 680	6944	36000000	50000	100	360000	8	[39]
adMSC[1]	1440	800	1.8	5000000	3472.20	45000000	31250	62.5	56250	11	[76]
bhMSC[2]	720	100	7.2	2250000	3125	43000000	59722.20	119.4444	430000	5	[57]
bhMSC[1]	1440	800	1.8	5000000	3472.20	110000000	76388.90	152.7778	137500	11	[76]
bhMSC[2]	3600	500	7.2	11250000	3125	160000000	44444.40	88.8888	320000	5	[57]
bhMSC[1]	5400000	2400	2250	15000000	2.8	670000000	124.1	0.2482	279166.70	11	[58]
bhMSC[1]	108000000	50000	2160	300000000	2.8	5900000000	54.6	0.1092	118000	11	[58]
hMSC[2,3]	450	90	5	2100 150	4667	27000000	60000	120	300000	5	[59]

[1]Performed using stirred tank bioreactor.

[2]Performed usingVWR.

[3]Tissue source not indicated.

SVR: growth surface to media volume ratio.

Cultures performed using iPS-MSCs, umbilical cord matrix-derived hMSCs (UCM-MSC), adipose-derived hMSCs (adMSC), and bone marrow-derived hMSCs (bhMSC) on collagen-coated polystyrene microcarriers (Pall Solohill or Corning Synthemax II) in vertical wheel bioreactors unless otherwise noted.